CORE
Metadata, citation and similar papers at core.ac.uk
Provided by Online Research Database In Technology

Technical University of Denmark

X-Ray Energy Dispersive Diffraction. Lecture Notes

Forskningscenter Risø, Roskilde

Publication date:
1988

Document Version
Publisher's PDF, also known as Version of record

Link back to DTU Orbit

Citation (APA):
Buras, B. (1988). X-Ray Energy Dispersive Diffraction. Lecture Notes. (Risø-M; No. 2151).

DTU Library
Technical Information Center of Denmark

General rights
Copyright and moral rights for the publications made accessible in the public portal are retained by the authors and/or other copyright owners and it is a condition of accessing publications that users recognise and abide by the legal requirements associated with these rights.

- Users may download and print one copy of any publication from the public portal for the purpose of private study or research.
- You may not further distribute the material or use it for any profit-making activity or commercial gain
- You may freely distribute the URL identifying the publication in the public portal

If you believe that this document breaches copyright please contact us providing details, and we will remove access to the work immediately and investigate your claim.

Risø-M-2751

RISØ

DK 8900262

Risø-M-2751

X-Ray Energy Dispersive Diffraction

Lecture Notes

Bronislaw Buras

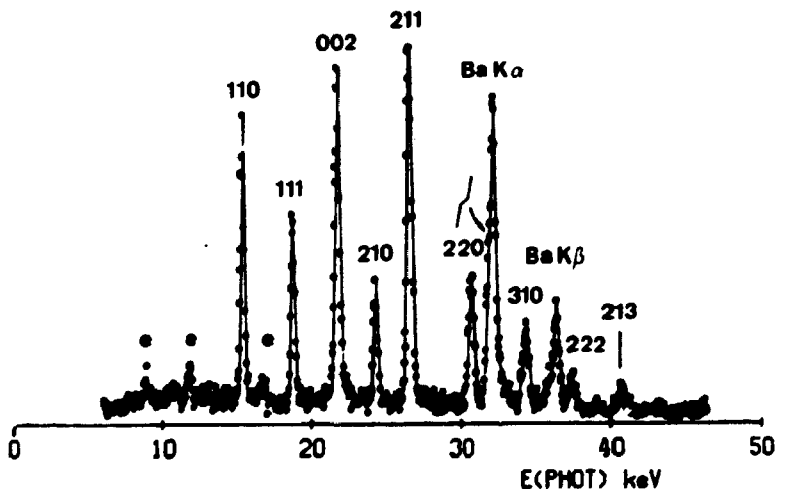

Risø National Laboratory, DK-4000 Roskilde, Denmark
October 1988

Risø-M-2751

X-ray energy dispersive diffraction

Lecture notes

Bronislaw Buras

Abstract

X-ray energy dispersive diffraction is used mainly for structural characterization of polycrystalline powders and amorphous materials. One of the important features of it is the fixed scattering angle facilitating in particular studies of materials in special environments (e.g., high pressure, high and low temperature). There are two versions of x-ray energy dispersive diffraction. In one - called XED - an incident "white" beam is used and the spectral distribution of the diffracted photons is analyzed by means of a solid state detector. Its important feature is the simultaneous appearance of all reflections. In the other version - called monochromator scan method (MSM) - the incident beam is monochromatic and its wavelength is changed stepwise by rotating the crystal monochromator.

The lecture notes describe both versions and present examples of their applications.

October 1988
Risø National Laboratory, DK-4000 Roskilde, Denmark

Nordisk Forskerkursus
Aarhus University and Sandbjerg Castle
19-26 August 1988

ISBN 87-550-1470-4
ISSN 0418-6435
Grafisk Service, Risø 1988

CONTENT

PREFACE

These lecture notes give a brief review of the X-ray energy-dispersive diffraction methods and presents several examples of its applications to structural studies of solids at high pressure and of amorphous materials. The review has an introductory character and does not pretend to be comprehensive. It is assumed that the reader is familiar with structural analysis of powdered crystals and amorphous materials performed by means of the monochromatic beam angular dispersive method.

The lecture notes are partly based on the review "Application of energy-dispersive diffraction for characterization of materials under high pressure" by B. Buras and L. Gerward to appear in "Progress in Crystal Growth and Characterization" edited by P. Krishna, Pergamon Press.

1. INTRODUCTION, THE XED AND MSM WHITE BEAM DIFFRACTION METHODS

There are two versions of the X-ray energy dispersive methods (Fig. 1). In both the scattering angle $2\theta_0$ is fixed. In the first version - called briefly XED - the beam impinging on the sample is a polychromatic ("white") one and the photon energy distribution of the scattered beam is analyzed by means of a solid state detector (SSD) connected to a multi-channel pulse height analyzer (Fig. 1a). One obtains an x-ray diffraction pattern: scattered intensity $I_0(E)$ versus photon energy E. An example of such a pattern is shown in Fig. 2.

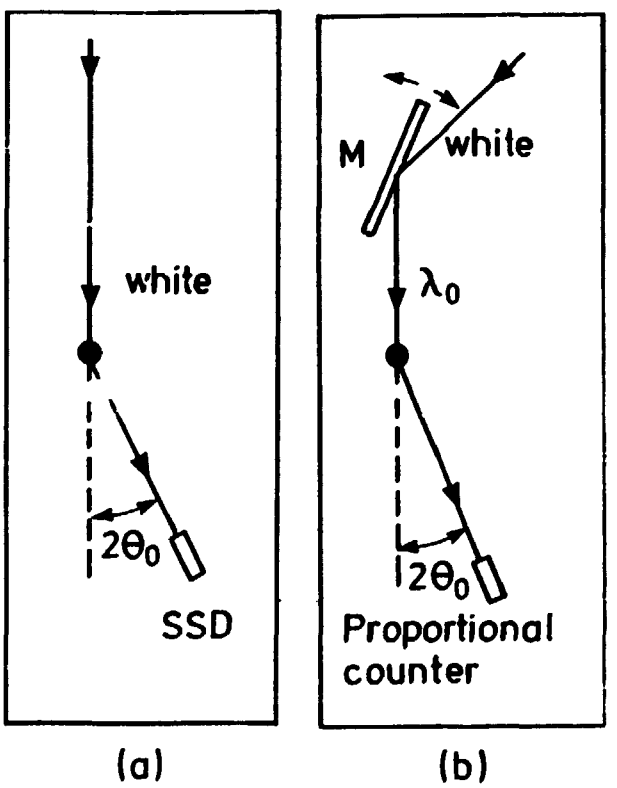

Fig. 1. X-ray energy dispersive powder methods: the XED method (a), and the MSM method. M - monochromator, S - polycrystalline sample.

In the second version - called monochromator scan method (MSM) - a monochromatic beam is impinging on the sample (Fig. 1b). Its wavelength (photon energy) is in the course of measurements changed step-by-step by rotating the monochromator. The intensity of the scattered X-rays is measured - separately for each photon energy - by a proportional counter. A SSD is not required. As a result one obtains an x-ray diffraction pattern: scattered intensity $I_o(E)$ versus photon energy E, similar to that given by XED.

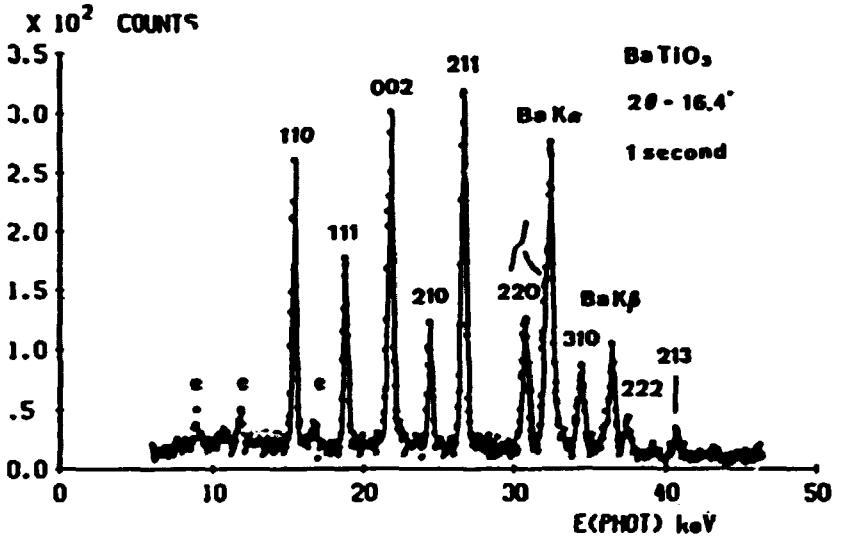

Fig. 2. XED diffraction pattern from $BaTiO_3$ powder recorded in 1 second at DORIS (3.7 GeV, 14 mA, E_c = 9.25 keV) with an ultra pure germanium detector.

It should be noted that both XED and MSM are in fact white beam methods, the difference being that in XED all photons present in the white beam are scattered simultaneously regardless of their energy, while in MSM they are scattered one-by-one depending on their energy. As a consequence the formula to be used in a crystal structure analysis is the same in both cases. For historical reasons they will be derived in conjunction with the description of the XED method.

The lecture notes discuss the XED method in some detail and MSM one only very briefly.

2. GENERAL INFORMATION ON XED

The method invented in 1968 [1,2]* is primarily applied to studies of polycrystalline samples and thus the following discussion is mainly devoted to this case. Structural studies of disordered materials are discussed in Section 7.

As already mentioned in the introduction and depicted in Fig. 1a the XED is a white beam method. Each set of crystal lattice planes of the powdered sample of spacing d_H (H indicates the Miller indices of reflection HKL) selects from the incident white spectrum photons of energy E_H (wavelength λ_H) fulfilling the Bragg equation

$$2d_H \sin\theta_o = \lambda_H = \frac{hc}{E_H} = \frac{12.398\,(\text{keV}\cdot\text{Å})}{E_H} \qquad (1a)$$

(h is Planck's constant, c the velocity of light), and reflects them into the detector. Figure 2 shows an example of a pattern measured at the synchrotron radiation source DORIS (Hasylab, Hamburg, FRG). The Bragg equation is usually written in a more convenient form for XED:

$$d_H \cdot E_H \cdot \sin\theta_o = C = 6.199\,(\text{keV}\cdot\text{Å}) \qquad (1b)$$

The integrated intensity of a reflection recorded by the detector along a unit length of the Debye-Scherrer ring is given by the formula

$$I_H = C[i_o(E)E^{-2}j|F|^2 \cdot \eta(E)A(E,\theta_o)C_p(E,\theta_o)]_H \sin^{-3}\theta_o \Delta\theta_o \qquad (2)$$

where C is a constant for a given experiment, $i_o(E)$ the incident beam intensity per unit energy range, j the multiplicity factor, F the structure factor including the atomic scattering factors and the temperature factors, $\eta(E)$ the detector quantum efficiency, $A(E,\theta_o)$ the attenuation factor, $C_p(E,\theta_o)$ the polarization factor and $\Delta\theta_o$ is a convolution of the incident and diffracted beams divergences. All values in the square bracket should be taken for the H reflection. The formula is derived in Sections 3 and 4.

From the positions E_H of the reflections in the energy scale, recorded by the solid state detector (see Fig. 1a), and the known scattering angle $2\theta_o$, one calculates a set of interplanar spacings d_H using eq. (1b). From the diffraction pattern, one calculates the integrated intensities I_H. Then by means of eq. 2 one can calculate a set of structure factors $[j|F|]_H$, provided that $[i_o(E), \eta(E), A(E,\theta_o), C_p(E,\theta_o)]_H$ are known. These factors are discussed in Sections 3 and 4.

With a set of interplanar spacings d_H and a set of structure factors $[j|F|]_H$ one may determine the structure of a given sample in the same way as in the case of the

* An annotated bibliography covering the years 1968-78 can be found in ref. [3].

angular dispersive method. The latter is described in great detail in the literature and thus is beyond the scope of these lecture notes.

The main characteristic features of the energy dispersive method differing from the x-ray monochromatic beam (angular scan) method, are the following:

(a) The incident beam is polychromatic ("white"),
(b) The scattering angle $2\theta_o$ is fixed during a measurement but can be optimized for each particular experiment. There is no mechanical movement during the recording.
(c) The detector is an energy-dispersive one,
(d) All reflections are recorded simultaneously,
(e) The counting time is relatively short due to the high detector efficiency and simultaneous recording of reflections.

There are many applications of the method. By far the most important are studies of structural transitions. In this case the simultaneous appearance of all reflections and the short exposure times are essential. The fixed geometry is very convenient when cryostats, furnaces or high pressure cells are used (only one inlet and one outlet window are necessary). XED is also very useful, among others, for structural studies of amorphous materials and textures, see sections 7 and 9.2, respectively.
A white (polychromatic) x-ray beam can be obtained from X-ray tubes (Bremsstrahlung) and from synchrotron radiation (SR) sources. The discussion in the present lecture notes is limited to SR. However, references are also made to experiments using x-ray tubes because each of these experiments could be made also with SR, though the opposite is not always true.

3. THE FORMULA FOR INTEGRATED INTENSITY FOR POLYCRYSTALLINE MATERIALS [1,4]

In the XED and MSM methods the relation between the integrated intensity and the structure factor is different from the one in the angular dispersive method. The basic formula valid for both XED and MSM is derived below within the framework of the kinematical theory of diffraction beginning with the classical formula for the power I^{cl}_H of a monochromatic beam of wavelength λ_o diffracted by a non-absorbing powder sample [4]. For the basic formula it is assumed also that both the efficiency of the detector and the attenuation factor are equal to 1. All corrections are included later. For the whole Debye-Scherrer ring we have

$$I^{cl}_H = r_o^2 \, i_o(\lambda)\Delta\lambda \, \frac{\lambda^3 \cdot j_H |F_H|^2}{4\sin\theta_B} \, C_p(E,\theta_B) \, \frac{\delta V}{V^2} \qquad (3)$$

where r_e is the classical electron radius, δV the sample volume, V the unit cell volume, θ_B is the Bragg angle and $\Delta\lambda$ the spectral width of the incident monochromatic radiation. The meaning of the other symbols was already explained in Section 1. The reason we write the polarization factor as $C_p(E,\theta_B)$ and not $(1+\cos^2 2\theta_e)/2$, as we do in the angular dispersive method, will become clear in Section 4.1. It should be noted that $i_e(\lambda)\Delta\lambda$ is the intensity of the incident beam usually denoted by I_e in the angular dispersive methods. In the latter methods $\Delta\lambda$ is defined either by the spectral width of the characteristic line or by the spectral width of the monochromatic beam obtained by means of a single crystal monochromator. In the white beam energy dispersive method $\Delta\lambda$ depends on the overall divergence $\Delta\theta_e$ of the incident and diffracted beams. By differentiation of the Bragg equation

$$2d\sin\theta = \lambda \tag{4}$$

with d constant one obtains

$$\Delta\lambda = \lambda \cdot \cot\theta \cdot \Delta\theta \tag{5}$$

and the formula for the integrated intensity in the white beam energy dispersive method is

$$I_H^e = r_e^2 \left| i_e(\lambda) \cdot \lambda^4 \, j \, |F|^2 \cdot C_p(E,\theta_e) \right|_H \frac{\cos\theta_e \cdot \Delta\theta_e \, \delta V}{4\sin^2\theta_e \, V^2} \tag{6}$$

for the whole Debye-Scherrer ring. All values in the bracket are taken for the H reflection.

If the detector of length ℓ (along the Debye-Scherrer ring) is located at distance R from the sample then the measured integrated intensity is $\ell/(2\pi R\sin 2\theta_e)$ times smaller and thus

$$I_H^e = \frac{r_e^2 \cdot \ell}{16\pi R} \left| i_e(\lambda)\lambda^4 j \cdot |F|^2 \cdot C_p(E,\theta_e) \right|_H \sin^{-3}\theta_e \frac{\delta V}{V^2} \Delta\theta_e \tag{7}$$

As mentioned in Section 1, the diffracted intensity is recorded as a function of photon energy. It is therefore convenient to express the integrated intensity in terms of the photon energy, which is related to the wavelength by the wellknown expression

$$E = \frac{hc}{\lambda} = \frac{12.4}{\lambda} \text{ (keV} \cdot \text{ Å)}. \tag{8}$$

The incident beam intensity per unit wavelength range, $i_0(\lambda)$, is related to the intensity per unit energy range, $i_0(E)$, through

$$i_o(\lambda) = i_o(E)\left|\frac{dE}{d\lambda}\right| = i_o(E)\frac{E^2}{hc} \tag{9}$$

From eqs. (7), (8) and (9) one has

$$I^o_H = C_o[i_o(E)E^{-2}]|F|^2 \quad C_p(E,\theta_o)|_H \sin^{-3}\theta_o \Delta\theta_o \tag{10}$$

where $C_o = (hc)^3 r_o \cdot \ell \cdot \delta V/(16\pi RV^2)$ is constant for a given experiment.

In order to obtain the full formula one must multiply I^o_H with a detector efficiency factor $\eta(E)$ and an attenuation factor $A(E,\theta_o)$. Finally one gets

$$I_H = C_o[i_o(E)E^{-2}]|F|^2\eta(E)A(E,\theta_o)C_p(E,\theta_o)|_H \sin^{-3}\theta_o \Delta\theta_o \tag{11}$$

For a given experimental set-up both θ_o and $\Delta\theta_o$ are constants and can be included into the constant C_o. One then obtains

$$I_H = C[i_o(E)E^{-2}]|F|^2 \cdot \eta(E)A(E,\theta_o)C_p(E,\theta_o)|_H \tag{12}$$

with

$$C = C_o \sin^{-3}\theta_o \cdot \Delta\theta_o . \tag{13}$$

It follows from the formula (12) that calculations of the structure factors from the measured integrated intensities require the knowledge of the spectral distribution $i_o(E)$ of the incident beam. It should be noted that for a fixed magnetic field bending the electron trajectory the spectral distribution of S.R. depends only on the electron energy. The fact that the spectral distribution is independent of the electron current is important because in a storage ring the current decreases with time. In the case of SR the spectrum $i_o(E)$ can be calculated in the first approximation from the storage ring parameters taking into account the attenuation of the beam by all materials which it penetrates on its way between the source and the sample. It can also be inferred e.g. from a diffraction pattern of a known sample.

4. CORRECTIONS TO THE FORMULA FOR INTEGRATED INTENSITY

4.1. Polarization Factor [5]

The polarization factor $C_p(E,\theta_o)$ depends obviously on the polarization of the incident beam, P(E), which is known to depend on the photon energy E. P(E) is defined with respect to a given plane as

$$P(E) = [i_{o,p}(E) - i_{o,n}(E)]/[i_{o,p}(E) + i_{o,n}(E)] \tag{14}$$

where $i_{o,p}(E)$ and $i_{o,n}(E)$ are the parallel and normal components of the incident beam intensity with respect to this plane.

When dealing with synchrotron radiation, the polarization P(E) is usually defined with respect to the plane of the electron orbit which is horizontal. Synchrotron radiation emitted by electrons on an ideal orbit is fully polarized, with the polarization vector in the plane of the electron orbit. In the case of a non-ideal electron orbit, the usual case, the radiation is not fully polarized in the orbital plane. However, the polarization P(E) can be calculated in the first approximation from the parameters of the storage ring. For more precise knowledge of the polarization it should be measured (see e.g. ref. 5b).

For an incident non-polarized beam, the polarization factor, as is well known, equals

$$C_p = \frac{1+\cos^2 2\theta_o}{2} \tag{15}$$

For an incident beam with a degree of polarization P(E) the polarization factor in the kinematical approximation equals [5a]

$$C_p(E,\theta_o) = \frac{1}{2}[1+\cos^2 2\theta_o - P(E)\cos 2\alpha \cdot \sin^2 2\theta_o] \tag{16}$$

where α is the angle between the plane defined by the incident and diffracted beam directions and the plane with respect to which the polarization P(E) was defined. In the case of synchrotron radiation the latter plane is horizontal and thus for scattering in this plane $\alpha = 0$ and

$$C_p(E,\theta_o)(\text{horizontal}) = \frac{1}{2}[1+\cos^2 2\theta_o - P(E)\sin^2 2\theta_o] \tag{17}$$

and for scattering in the vertical plane $\alpha = 90°$ and

$$C_p(E,\theta_o)(\text{vertical}) = \frac{1}{2}[1+\cos^2 2\theta_o + P(E)\sin^2 2\theta_o]. \tag{18}$$

As mentioned above in the case of a storage ring P(E) can be calculated and thus also $C_p(E,\theta_o)$. When no great precision is required one can assume that $P(E) \approx 1$ and thus

$$C_p(E,\theta_o)(\text{horizontal}) \approx \cos^2 2\theta_o \tag{19}$$

$$C_p(E,\theta_o)(\text{vertical}) \approx 1 \tag{20}$$

As shown in Fig. 3 there exists in the case of a horizontal scattering plane a "blind" region around $2\theta° = 90°$. A vertical scattering plane is much more

favourable because for all energies and all scattering angles $C_p(E,\theta_o)$(vertical) ≈ 1. However, the mechanical construction of the diffractometer, mounting of furnaces, cryogenic equipment etc. are easier to handle when the x-rays are scattered in the horizontal plane.

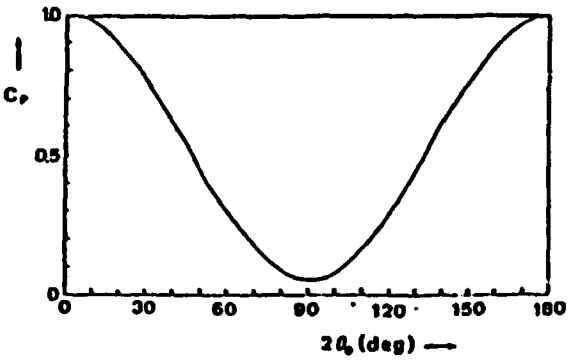

Fig. 3. The polarization factor $C_p(E,\theta_c)$ for a powdered sample calculated for a horizontal scattering plane and an ideal electron orbit.

It has been shown [5a] that the beam can be treated as unpolarized when the angle between the scattering plane and the plane of the electron orbit is 45°.

4.2. Attenuation factor $A(E,\theta_o)$

Well established methods and formulas exist for calculating the attenuation factor for the monochromatic beam angular dispersive method. In the energy-dispersive method the photon energy (wavelength) changes from reflection to reflection and thus one calculates the attenuation factor separately for each reflection using the above mentioned methods and formulas. As a consequence, the attenuation factor is a function both of photon energy and scattering angle. In the calculations one can use within a good approximation the energy corresponding to the peak position. Attention should be called to the fact that changes of the absorption as function of photon energy are rather dramatic, in particular at absorption edges.

4.3. Solid state detectors; callibration; quantum efficiency [6]

A solid state detector transforms the energy of an absorbed photon into an electrical pulse of height proportional to the photon energy. These pulses are sorted out according to their height by a multichannel pulse height analyzer. Each channel number corresponds to a defined energy. Thus in general the measured photon energy E is a function of the channel number N.

This function is determined by a callibration procedure using the photon energies of characteristic radiation of several elements excited by a radioactive source. An example of the result of such callibration procedure is shown in Fig. 4.

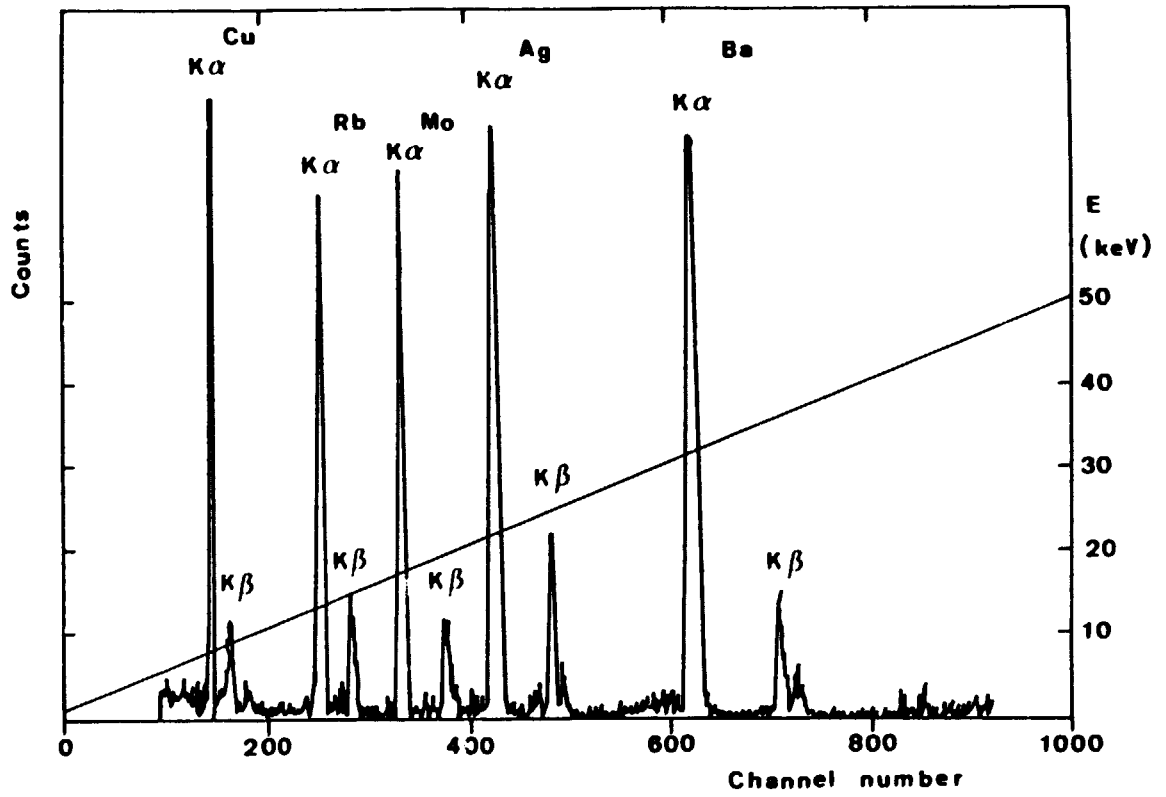

Fig. 4. An example of the result of calibration of a multichannel pulse-height analyzer using the known photon energies of characteristic radiation of Cu, Rb, Mo, Ag and Ba.

The detectors usually used are high purity germanium (HPGe) and Si(Li). The Lithium drifted detectors must be kept at liquid nitrogen temperature all the time. The extra pure Ge detector must be at liquid nitrogen temperature only during the measurements. The detectors have a build-in low noise preamplifier kept at the same temperature as the detector. The preamplifier is connected to a multichannel pulse height analyzer through an amplifier. The data can be displayed on a fluorescent screen or on an X-Y plotter and recorded on a magnetic tape. They can also be directly transferred to the memory of a computer for data treatment.

There are two important characteristics of semiconductor detectors: (i) energy resolution and (ii) quantum efficiency $\eta(E)$. The energy resolution is discussed in Section 5. The efficiencies are illustrated in Fig. 5. One sees that the Si(Li) detector has a quantum efficiency of unity for low energy photons, but drops rapidly for photons above 30 keV. It should be noted also that the efficiency curve is a smooth one. In the case of a Ge detector, the high efficiency extends to higher photon energies. However, the efficiency curve in this case has a kink at 11.1 keV due to the absorption K-edge in Germanium. As a consequence, it is difficult to estimate the spectral distribution $i_0(E)$ in the region of about 11 keV. For reasons of both high efficiency and smoothness of the efficiency curve the Si(Li) detectors are used for low energy photons, say, up to 30 keV and Ge detectors for high energy photons above ~ 12 keV.

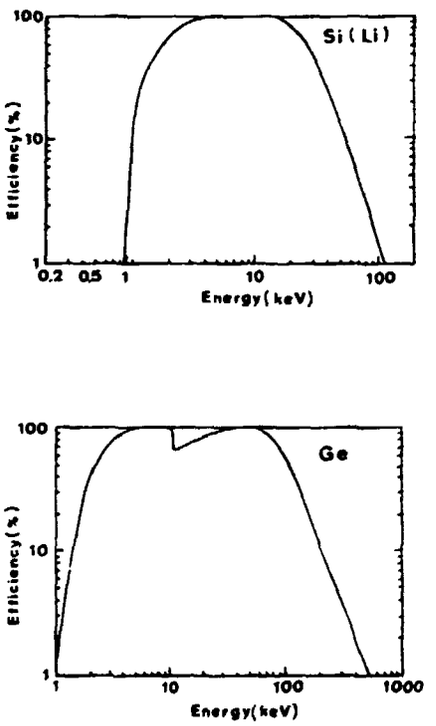

Fig. 5. Quantum efficiency of semiconductor detectors as function of photon energy.

5. EXPERIMENTAL SET UP [7-9]

The principal elements of an experimental set up were already shown in Fig. 1. More details of a set-up at a SR source are shown in Fig. 6. (Examples of existing XED diffractometers are among others described in Refs. 7-9). The directions and divergences of the incident and diffracted beams are defined by slits S_1, S_2 and S_3, S_4, respectively. They also define the mean scattering angle $2\theta_0$. For small samples (e.g. 0.3 mm in diameter) slit S_3 may usually be omitted.

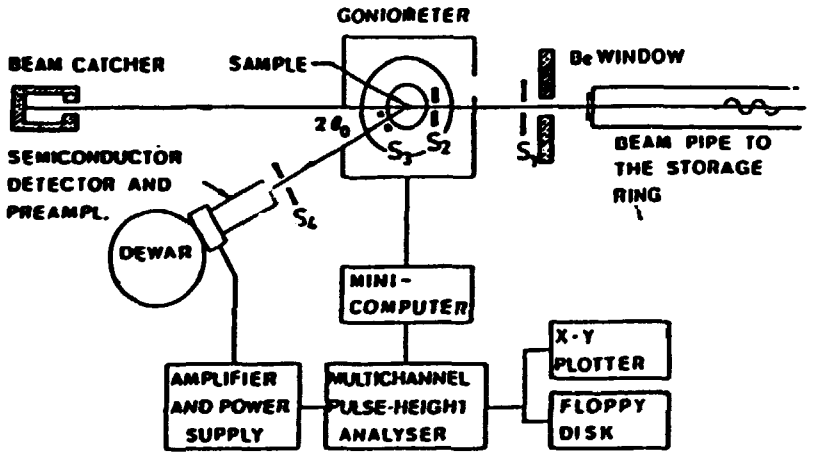

Fig. 6. An XED set-up at a SR source (schematically).

The divergences of the incident and diffracted beams depend on the widths of the slits and the source-sample and sample-detector distances, respectively.

The source-sample distance depends on the storage ring and the location of the experiment in the experimental hall. It varies, say, from 10 m to 40 m. The sample-detector distance is much smaller, usually below 1 m. As a consequence, the widths of the slits for the diffracted beam must be much smaller than for the incident beam.

The dimensions of the source in a storage ring varies from several millimeters to parts of a millimeter. Table 1 presents, as examples, the FWHM's of the

dimensions of S.R. sources from bending magnets of DORIS and the expected ones of the European Synchrotron Radiation Facility (ESRF).

Table 1. Full widths at half maximum of S.R. sources (in mm)

	DORIS	ESRF expected
Horizontal plane	2.4	0.4
Vertical plane	0.7	0.3

Due to these small source sizes, the slit 1 (see Fig. 6) is in many cases superfluous*). Assume, for example, a source size of 1 mm, the width of slit S_2 equals 0.2 mm and the source-sample distance is 20 m. Then the divergence of the incident beam is 10^{-4} radians. For the diffracted beam it is difficult to obtain such a small divergence. For a rather large 1 m distance between the sample and the detector and slits S_3 and S_4 of widths 0.1 mm each, one obtains a divergence of $2 \cdot 10^{-4}$ radians. At present S.R. sources this may lead to insufficient intensity. At the ESRF it should not involve any problems.

As will follow from the next section, for Bragg angles larger than, say, 10 degrees a divergence of the order mentioned above gives only a small contribution to the overall resolution governed mainly by the energy resolution of the SSD detector.

The recording time depends clearly on the number of photons per second passing the solid angle defined by the source size and slit S_2. Thus the figure of merit of an SR source for XED is brightness.

In order to reduce the background appropriate shielding must be used. In case of S.R. for safety reasons the whole experimental set-up is placed in a hatch covered with lead (~ 5 mm thick). Thus all movements of the detector, sample and

*) One should use, however, a diaphragm in order to reduce the background.

goniometer must be remotely controlled. An important element of such a set-up is the beam catcher (see Fig. 6).

6. PRECISION OF THE XED METHOD

By differentiation of the Bragg equation 1b and under the assumption that errors δE and $\delta\theta_o$ of the measurements of photon energy and Bragg angle, respectively, are of a statistical nature, one obtains

$$\frac{\delta d}{d} = \left[\left(\frac{\delta E}{E}\right)^2 + \left(\cot\theta_o \delta\theta_o\right)^2\right]^{1/2} \tag{21}$$

where δd is the absolute precision of the interplanar spacing measurement.

$\delta\theta_o$ is usually 5 millidegree $\approx 10^{-4}$ radians or smaller. As we shall see later, θ_o is seldom smaller than 5° and thus $\cot\theta_o\delta\theta_o$ is usually smaller than 10^{-3}.

In order to calculate δE it is necessary to consider two values: the energy resolution δE_D of the detector system and δE_θ, the energy broadening of the reflection due to beam divergence. Following Ref. 10 we have

$$\delta E_D = [(\Delta E_{amp})^2 + 5.546\, F \epsilon\, E]^{1/2} \tag{22}$$

where ΔE_{amp} is due to the dark current through the solid state detector and to the noise in the field-effect transistor and the preamplifier, F is the Fano factor, ϵ is the energy required for creating an electron-hole pair. δE_θ we get by differatiating the Bragg equation with d = const

$$\delta E_\theta = -E \cot\theta_o \Delta\theta_o \tag{23}$$

where $\Delta\theta_o$ is the beam divergence. Assuming a Gaussian distribution for both δE_D and δE_θ one obtains

$$\delta E = [(\delta E_D)^2 + (\delta E_\theta)^2]^{1/2} \tag{24}$$

Simple algebra then gives

$$\frac{\delta E}{E} = C^{-1}[(\Delta E_{amp} \cdot d \cdot \sin\theta_o)^2 + 5.546 \cdot CF\epsilon d \sin\theta_o + (C\cot\theta_i \Delta\theta_\theta)^2]^{1/2} \tag{25}$$

with C = 6.199 keV Å.

Fig. 7 shows examples of the dependence of $\delta E/E$ on θ_o for two interplanar spacings 0.5 Å and 1 Å and two divergences 10^{-4} and 10^{-3} radians. Note that in all four cases $\delta E/E$ decreases with decreasing θ_o down to a certain minimum and

then increases rapidly. The initial decrease is due to the first term in Eq. 25, however, when θ_0 becomes very small the leading term is the last one, which blows up for small θ_0. Fig. 7 illustrates also that $\delta E/E$ decreases with decreasing interplanar spacing, and that the minimum value of $\delta E/E$ is smaller for smaller d and shifts to smaller θ_0. A small θ_0 for a given lattice spacing means a large photon energy.

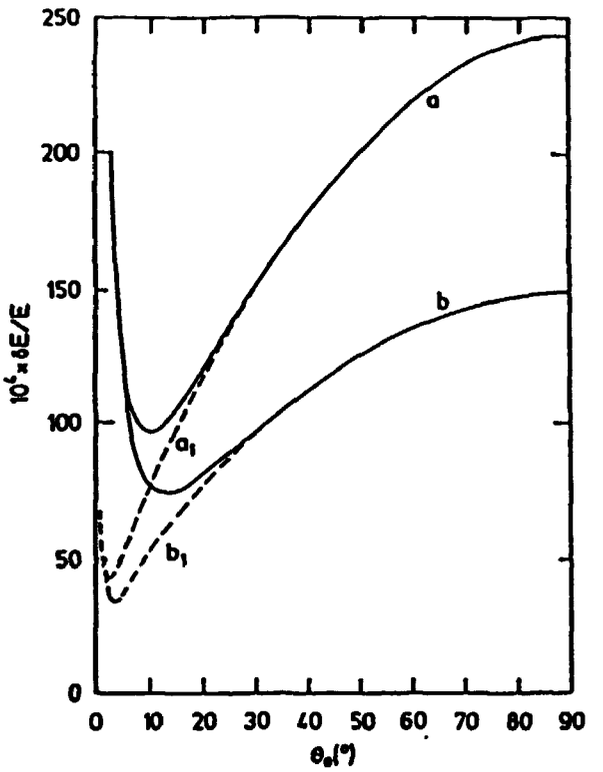

Fig. 7. $\delta E/E$ as function of θ_0 for two interplanar spacings: 1 Å (curve a) and 0.5 Å (curve b). The full lines are for $\Delta\theta_0 = 10^{-3}$, the dotted for $\Delta\theta_0 = 10^{-4}$.

Using formulas 25 and 26 one obtains

$$\frac{\delta d}{d} = C^{-1}\{(\Delta E_{amp} \cdot d \cdot \sin\theta_0)^2 + 5.546 \cdot CF\epsilon \sin\theta_0 + [\cos\theta_0(\Delta\theta_0 + \delta\theta_0)]^2\}^{1/2} \qquad (26)$$

It follows from Fig. 7 that for $\Delta\theta_0 = 10^{-4}$ radians - which it is possible to achieve with SR - and angles, say, smaller than 10° (but not too small) $\delta E/E$ is smaller than 10^{-2}. It should, however, be recalled that δE is the full width at half

maximum and that the centroid of the reflection can be measured with a precision, say, 10 times or more better. Thus the $\delta E/E$ value in Eq. 21 can be made smaller than 10^{-3} and thus of the same order as $\cot\theta_0\delta\theta_0$. In conclusion, $\delta d/d$ can be measured with a precision of 10^{-3} or better for the condition mentioned above. However this involves high energy photons.

Fig. 8 shows an example of an improvement of energy resolving power by increasing the photon energy. One easily notices that although δE increases with photon energy, the distance between the reflections increases faster and they are better separated.

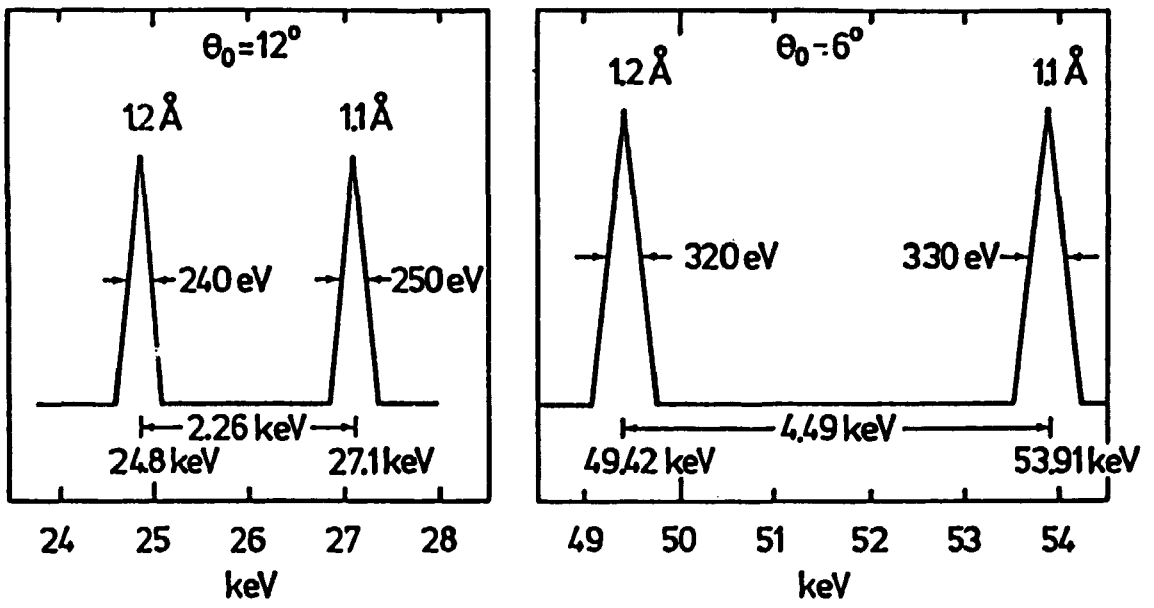

Fig. 8. An example of an improvement of energy resolving power by decreasing the scattering angle.

In conclusion one sees that high energy photons improve both the accuracy of lattice spacing measurements and the resolving power.

To get an idea of the required photon energies we assume $\Delta\theta_o = 10^{-4}$ and $\theta_o = 5$ which is close to the value of θ_o leading to small $\delta E/E$ for d = 0.5 Å. In this case E = 142 keV. Wavelengths shifters can easily emit photons of this energy, however the efficiency of the Ge solid state detector decreases several times (see Fig. 4). Due to the high intensity of modern S.R. sources, this should not cause any problems in most cases one can think of.

The accuracy of structure factor determination depends - in addition to accuracy with which E can be measured - on the accuracy with which the incident intensity and the attenuation, polarization and detector efficiency factors (see Eq. 2) can be estimated. Also, the energy dependent Compton effect should be taken into account. All these lead in practice to the conclusion that in general the XED is a less precise method for structure determination than the monochromatic beam angular method. However, its other qualities enumerated in Section 1 make the XED a useful and convenient method in many cases. Some applications are briefly described in the section 9.

7. STRUCTURAL STUDIES OF AMORPHOUS MATERIALS

The use of XED for structural studies of amorphous materials is illustrated with the simple example of a monoatomic amorphous material.

As is well known, the structure of an amorphous monoatomic material is characterized by the radial distribution function (RDF) $4\pi r^2\rho(r)$, where $\rho(r)$ is the number density of the material at a distance r from an atom placed at the origin (r=0). The scattered intensity is denoted $I_o(q)$, where $q = (4\pi\sin\theta)/\lambda$ is the modulus of the scattering vector. After correcting $I_o(q)$ for the incident spectrum, absorption, polarization, Compton scattering etc. one obtains I(q). It can be shown that

$$qI(q) = \int_0^\infty 4\pi r^2 [\rho(r) - \rho_o] \sin qr \tag{27}$$

where ρ_o is the average number density. After Fourier transformation, this yields

$$4\pi r^2 [\rho(r) - \rho_o) = (2/\pi) \int_0^\infty qI(q) \sin(qr)\, dq \tag{28}$$

$I_o(q)$ and I(q) are usually continuous oscillating functions (see Fig. 9a,b). The widths of the peaks are broad and thus very good accuracy in determining the positions of the peaks is not required. However, the Fourier transform (see Fig. 9c) is very sensitive to the shape of I(q). In the angular dispersive method one

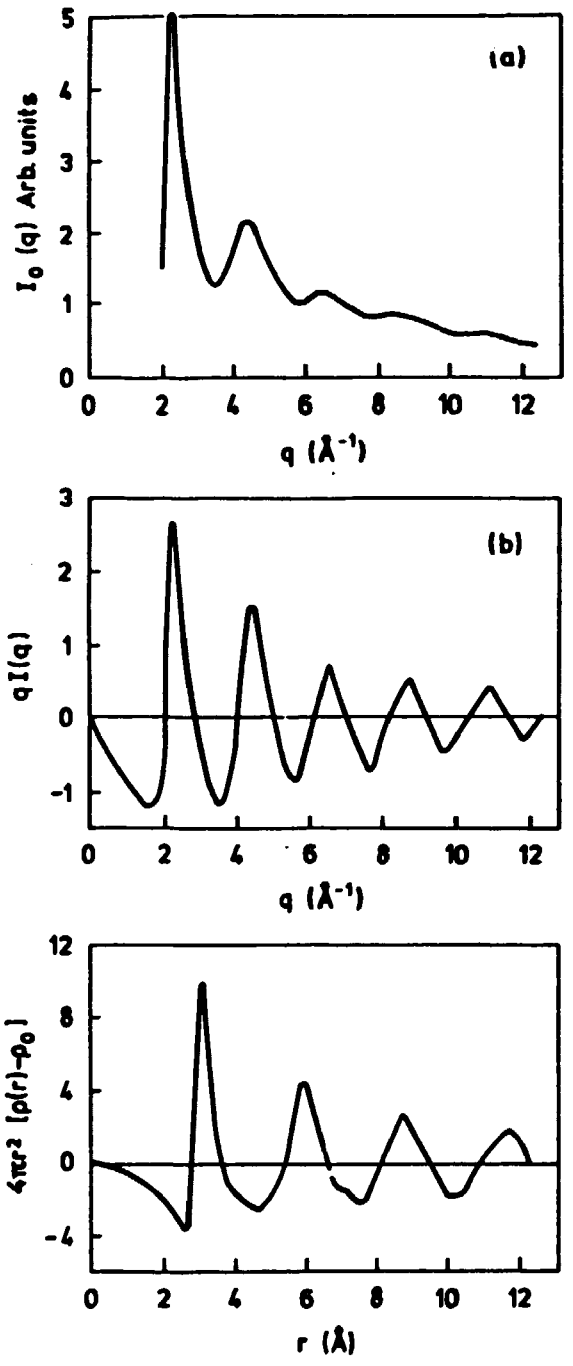

Fig. 9. The measured (a) intensity $I_o(q)$ of the beam scattered by an amorphous material (mercury) versus scattering vector q, (b) the corrected intensity I(q) - see text, (c) the RDF versus distance from an atom placed at the origin. After Ref. 20.

measures $I_o(q)$ consecutively point by point by changing stepwise the scattering angle. It follows from the above that the steps must be small and thus the measurements are time consuming*).

In the XED $q = (4\pi/hc)E \cdot \sin\theta_o \approx 1.01\ E\sin\theta(\text{Å}^{-1}/\text{keV})$ and the steps of q depend on the steps of E, which are determined by the chosen channel width of the multichannel pulse-height analyser. It can be made very small. In conclusion: by means of XED the shape of I(q) is measured simultaneously for a desired range of q and with a better accuracy than in the angular dispersive method. This may explain the fact that a relatively small amount of work on amorphous materials has been done prior to the development of XED.

8. THE MONOCHROMATOR SCAN METHOD (MSM)

We introduce the method by presenting the monochromator scan diffractometer recently described by Parish and Hart (1987) (Fig. 10). An X-ray white beam from a storage ring is defined by slit C and diffracted by Silicon (111) double crystal monochromator mounted on the diffractometer D_1. The monochromatic beam,

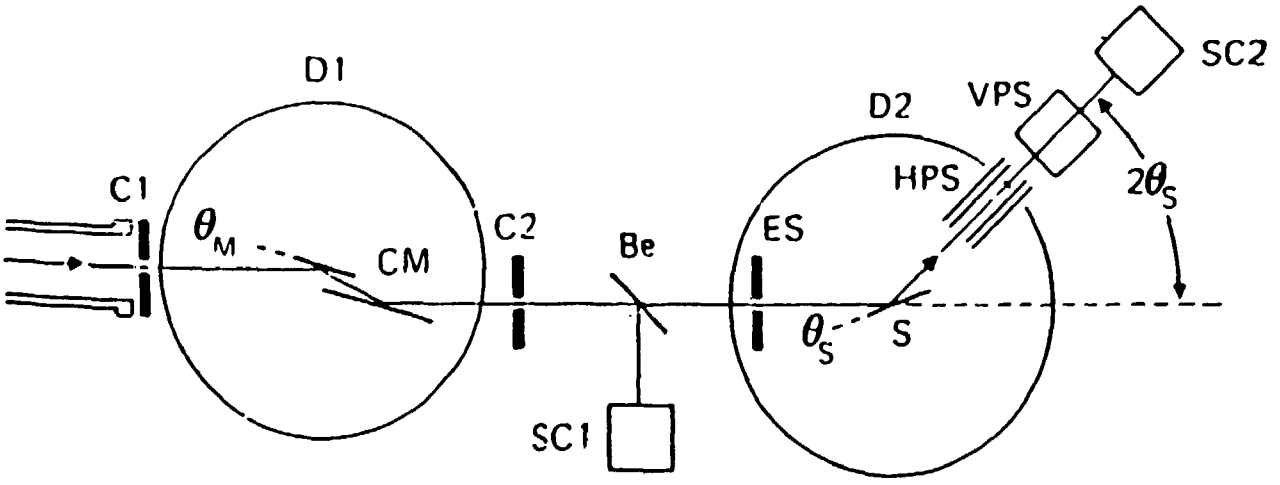

Fig. 10. Experimental set-up for energy dispersive diffraction by means of a monochromator scan. The symbols are explained in the text. (After Ref. 11).

*) This situation has recently changed with the development of position-sensitive detectors.

which wavelength depends on the Bragg angle θ_M, is directed to the sample S using the slits C2 and ES. The instrumentation is designed so that any wavelength can be used without realigning the second diffractometer D2 used for the sample. The monochromatic beam is monitored by measuring the scattering from a thin (0.025 mm) inclined Be foil with a scintilation counter SC1. The monitor counts are used to normalized the measured data to a constant intensity of the monochromatic beam impinging the sample. The intensity of the beam diffracted by the powdered sample under a fixed angle θ_s is measured by a proportional counter.

In the course of the experiment the monochromator is turned in small steps and consequently the wavelength of the radiation incident on the sample also changes accordingly. As a result one obtains an x-ray pattern of the same kind as using the XED method. An example of such a pattern obtained by means of the MSM method is shown in Fig. 11.

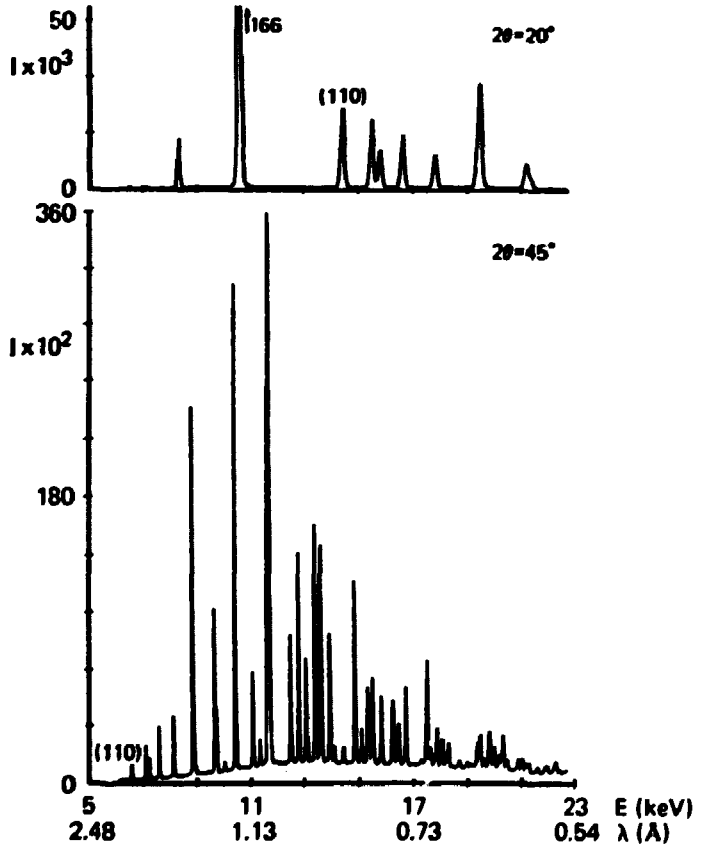

Fig. 11. Energy dispersive diffraction pattern of quartz with the same energy range (5-23 keV) but different 2θ settings. The (110) reflection is marked in both patterns for comparison. The intensities at the longer wavelength are reduced by air absorption. (After Ref. 11).

In both methods - the XED and MSM - the scattering angle is fixed which is of great advantage in particular for experiments with samples in special environments. In the XED, as opposed to the MSM, all reflections are recorded simultaneously, which is of great importance for phase transition studies. One should also notice that in the XED experimental set-up there are no moving parts as opposed to the MSM. However, the resolving power of MSM is in general better than that of XED.

9. APPLICATIONS

9.1. Introduction

The XED found many applications in material sciences, however, the main interest lies within two broad areas. The first involves structural studies and phase transitions at high pressures and high (low) temperatures. The second involves structural studies of amorphous materials including crystallization phenomena. However, one can find also applications of XED in other fields, as for example, studies of texture in thin films [12,13], anharmonicity [14], measurements of mean-square atom displacements [15], and others. Both Bremstrahlung from x-ray tubes and synchrotron radiation are in use.

9.2. Textures

In an ideal polycrystalline material the directions of crystallographic planes is isotropically distributed in space. However, e.g. rolling of a polycrystalline material can create a preferred orientation of crystallographic planes (socalled texture). As a result the properties of the material, e.g. strength, may become different in different directions. Thus the knowledge of texture is important for some applications of polycrystalline materials. It can be revealed and measured by x-ray and neutron scattering. Figure 12a shows an XED diffraction pattern of iron along the rolling direction, and Fig. 12b perpendicular to it. From the intensities of the reflections (011) and (002) one easily conclude that the crystallographic planes (002) are lying almost predominantly in the rolling direction, while the (011) planes are predominantly perpendicular to the rolling direction. The simultaneous appearance of all reflections, characteristic for XED, is essential for such measurements.

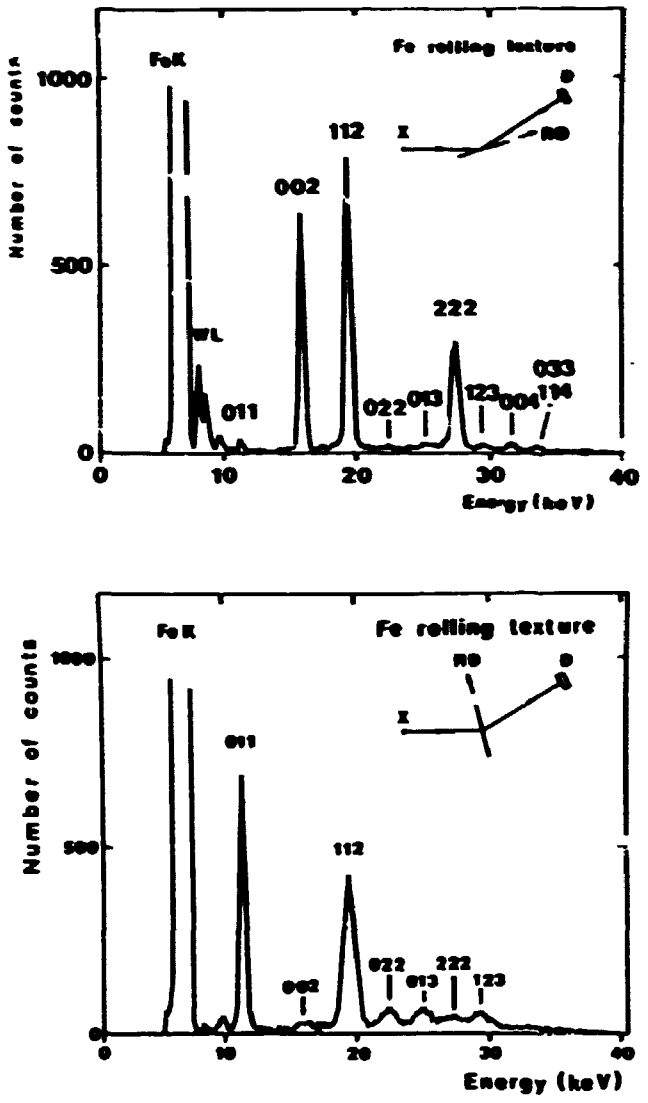

Fig. 12. An XED diffraction pattern from iron along the rolling direction (a), and perpendicular to the rolling direction. (Leif Gerward, private communication).

9.3. Structural Studies at High Pressures [17-21]

In recent years structural studies of solids under high (tens and hundreds of kilobars) and very high (megabars) pressures have become increasingly important for basic and applied solid state physics and geophysics [17]. The high and very high static pressures are obtained by means of diamond-anvil cells DAC (see e.g. Ref. 18) and the most frequently used diffraction method is XED.

Fig. 13 shows the principle of a DAC cell. The sample is placed in a small hole in a 0.1-0.3 mm thick metal foil (gasket). The pressure is exerted by the two flat diamond faces pressed against each other. The volume of the sample is very small

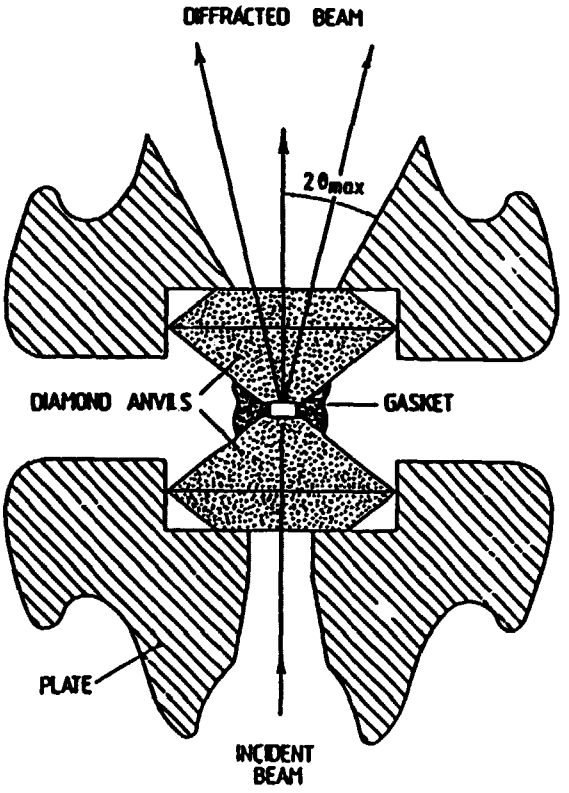

Fig. 13. The diamond anvil high pressure cell - schematically. See text.

(10^{-5}-10^{-3} mm^3) and thus for structural studies a high brightness x-ray source is needed. Although x-ray tubes can be used SR presents a great challenge. The DAC is placed on the sample table of an XED diffractometer mentioned in Section 5 and described in some detail in Ref. 7-9.

As an example of such studies we discussed the pressure induced transformation of YbH_2 at room temperature [19]. The structure of this material at atmospheric pressure is orthorhombic. The XED diffraction patterns at four different pressures are presented in Fig. 14. It is clearly seen that at 14.3 GPa (143 kbar) some new reflections appear in addition to those characterizing the orthorhombic structure. At 17.0 GPa the reflections from the orthorhombic structure have partly disappeared, and at 28.2 GPa they are absent. On the basis of the measured interplanar spacings the high pressure structure was identified as

hexagonal. The orthorhombic phase can be viewed as a distorted hexagonal packing with c/a ≈ 1.6, and the transformation as a collapse to a hexagonal structure with c/a = 1.34.

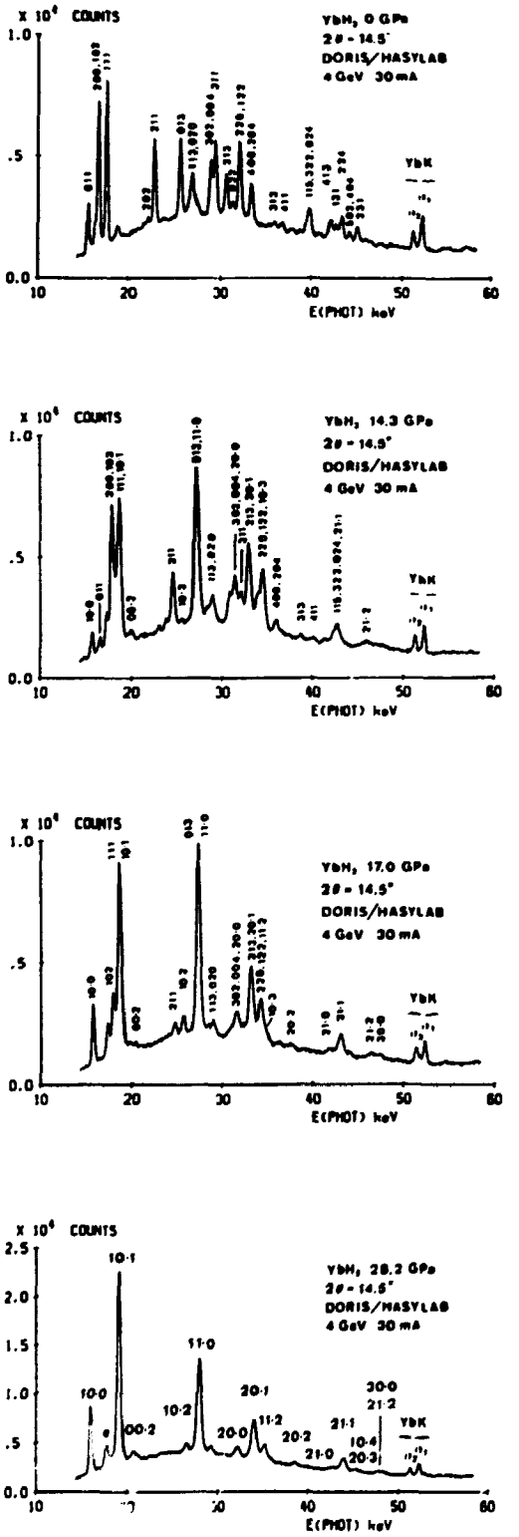

Fig. 14. The XED diffraction pattern of YbH_2 at several pressures. (After Ref. 19).

This example illustrates clearly the ability of studies of phase transformation in situ, recording the transformation step by step with changing pressure. The equation of state for a particular phase can be determined by measuring the unit cell volume as a function of pressure (an example is given in Ref. 18). Quantitatively, the equation of state can be used to calculate material parameters, such as the bulk modulus and its pressure derivative.

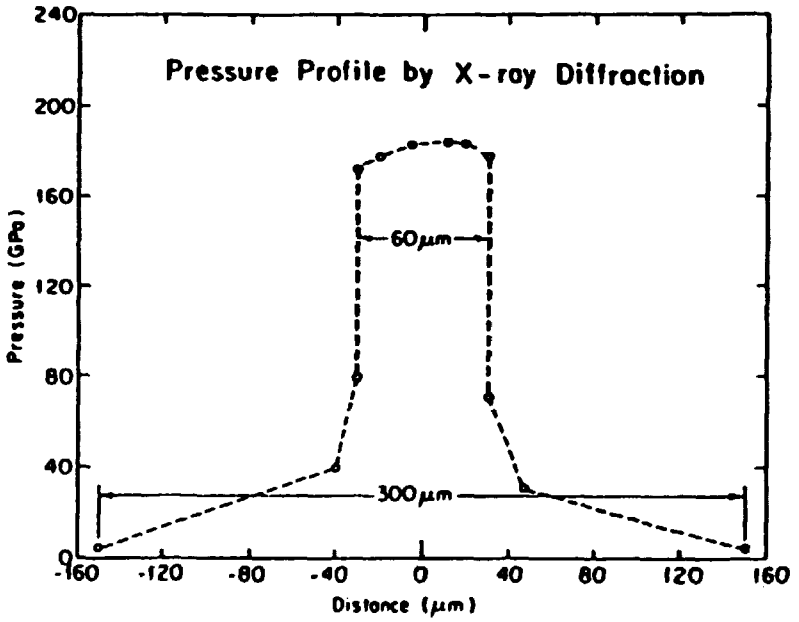

Fig. 15. The pressure profile on the rhenium gasket measured by XED from the measured volume of the hcp unit cell of Re-metal at various locations. The distances shown are measured with respect to the center of the diamond or the highest pressure region in the cell. (After Ref. 21).

Another example illustrates structure studies at ultra-high pressures [21], where XED and SR were used to study Re-metal up to 2.16 Mbar (216 GPa). It was found that the hcp structure exists up to this pressure (volume fraction $v/v_0 = 0.734$) and the c/a ratio is independent of pressure. In this study the x-rays were also used to obtain a pressure profile across the diamond face (Fig. 15). This required a very narrow beam of a very high intensity.

9.4. Structural Studies of Disordered Materials

For disordered materials (e.g. amorphous metals, amorphous polymers, liquids) the determination of the pair correlation function or the radial distribution

function are of primary importance. As already mentioned, the angle dispersive method is in this case difficult and time consuming. In contrast the XED enables a much faster and more accurate determination of the radial distribution function. Examples of such studies can be found in Ref. 22-24.

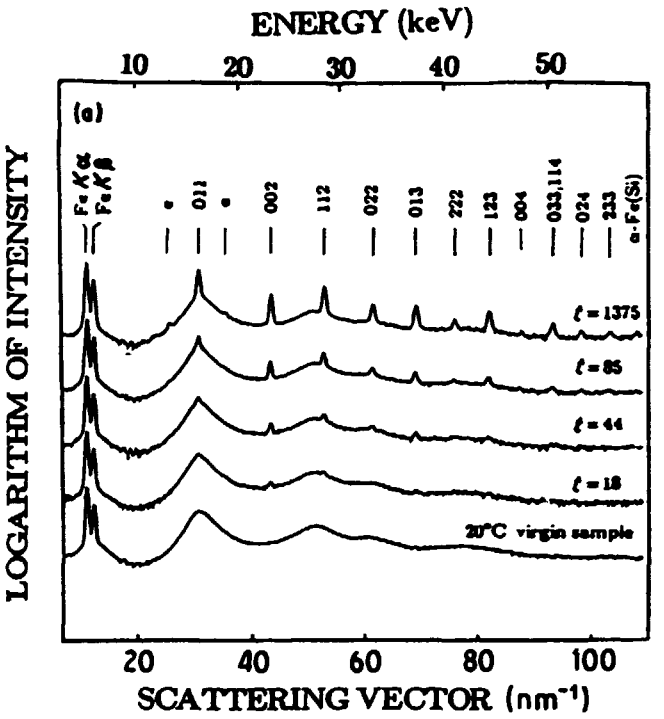

Fig. 16. Series of diffraction patterns of the crystallization of $Fe_{83}Si_7B_{10}$ after annealing at 350°C for 18, 44, 85 and 1375 minutes. The pattern of the virgin amorphous sample at room temperature is also shown. (After Ref. 25).

9.5. Crystallization of Metallic Glasses

Metallic glasses have attracted much interest due to their remarkable magnetic and mechanical properties. Because the amorphous state is metastable it can be transformed to a crystalline one by annealing at elevated temperatures. These studies are interesting from a scientific point of view and are also important for practical applications of metallic glasses. As an example, we briefly present the work on crystallization of Fe-Si-B [25]. Amorphous ribbons of $Fe_{90-x}Si_xB_{10}$ with x ranging from 7 to 21 were investigated using XED and S.R. at DORIS at Hasylab/DESY. The samples were placed in a special furnace and could be heated up to several hundred degrees C. The annealing was isothermal. The temperature was raised to the desired value and then the structural changes as a function of time were studied by means of XED. The counting time was several minutes.

Then the temperature was raised and again the structural changes were measured as a function of time. Fig. 16 shows an example of a diffraction pattern obtained in case of $x = 7$. By analysing the patterns it was possible to study the

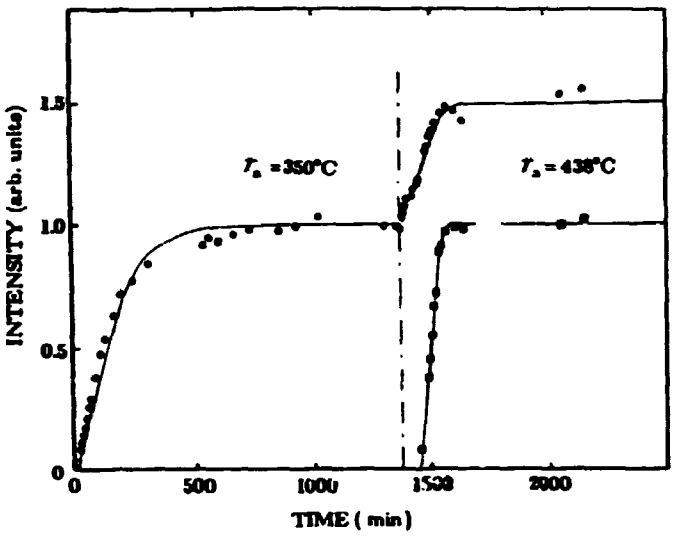

Fig. 17. The time-dependence of the integrated intensity of (o, •) the (0 0 2) peak of α-Fe(Si) and (■) the (0 2 2), (1 3 0) peaks of Fe_2B of $Fe_{83}Si_7B_{10}$ during annealing. The left-hand side of the figure shows annealing at 350°C and the right-hand side shows continued annealing at 438°C. (After Ref. 25).

time dependence of the evolving new phase and identify its crystallographic structure. The latter was done mainly by examination of the peak positions and comparing the interplanar spacings found in this way with the ones of known chemical compounds of iron, silicon and boron. In the case of $x = 7$ it was found that the new phases are α-Fe(Si) and Fe_2B. Fig. 17 shows the time dependence of the integrated intensities of the evolving two phases at two different temperatures.

---ooOoo---

The author expresses his thanks to Dr. Leif Gerward and Dr. Bente Lebech for reading the manuscript and useful comments.

REFERENCES

1. Buras, B., Chwaszczewska, J., and Szmid, Z. (1968). Fixed angle scattering (FAS) method for x-ray crystal structure analysis. Institute of Nuclear Research, Warsaw, Report No. 894/II/PS, 10 pp.

2. Giessen, B.C. and Gordon, G.E. (1968). X-ray diffraction: New high-speed technique based on x-ray spectroscopy. Science 159, 973-975.

3. Laine, E. and Lahteenmaki, I. (1980). The nergy dispersive x-ray diffraction method: annotated bibliography 1968-1978. J. Mater. Sci. 15, 296.

4. Buras, B. and Gerward, L. (1975). Relations between integrated intensities in crystal diffraction methods for x-rays and neutrons. Acta Cryst. A31, 372-374, and references therein.

5a. Olsen, J. Staun, Buras, B., Jensen, T., Alstrup, O., Gerward, L. and Selsmark, B. (1978). Influence of polarization of the incident beam on integrated intensities in x-ray energy-dispersive diffractometry. Acta Cryst. A34, 84-87.

5b. Templeton, D.H. and Templeton, L.K. (1988). Polarization of synchrotron radiation. Appl. Cryst. 21, 151-153.

6. Worgan, J.S. (1982). Energy dispersive detectors for synchrotron radiation. Nucl. Instrum. Methods 201, 85-91.

7. Olsen, J. Staun, Buras, B., Gerward, L. and Steenstrup, S. (1981). A spectrometer for x-ray energy-dispersive diffraction using synchrotron radiation. J. Phys. E: Scient. Instrum. 14, 1154-1158.

8. Skelton, E.F., Qadri, S.B., Webb, A.W., Lee, C.W. and Kirkland, J.P. (1983). Improved system for energy-dispersive x-ray diffraction with synchrotron radiation. Rev. Sci. Instruments 54, 403-409.

9. Brister, K.E., Vohra, Y.K. and Ruoff, A.L. (1986). Microcollimated energy-dispersive x-ray diffraction apparatus for studies at megabar pressures with a synchrotron source. Rev. Sci. Instrum. 57, 2550-2563.

10. Buras, B., Niimura, N. and Olsen, J. Staun (1978). Optimum resolution in x-ray energy dispersive diffractometry. J. Appl. Cryst. 11, 137-140 and references therein.

11. Parish, W. and Hart, M. (1987). Advantages of Synchrotron Radiation for Polycrystalline Diffractometry. Z. für Kristallography 179, 161-173.

12. Hariuchi, T., Fukao, K., Matsushige, K. (1987). New evaluation method of evaporated organic thin films by energy dispersive x-ray diffractometer. Jpn. J. Appl. Phys. 26, L 1839-41.

13. Hart, M. Parish, W., Masciocchi, N. (1987). Studies of texture in thin films using synchrotron radiation and energy dispersive diffraction. App. Phys. Lett. (USA) 50, 897-9.

14. Tranguda, J.M., Trautman, C., Heald, S.M. (1987). X-ray diffraction study of anharmonicity in V_3Si. Phys. Rev. B 35, 4193-8.

15. Metzger, T.H. (1986). An energy-dispersive x-ray diffraction study of mean-square atom displacements in highly oriented pyrolytic graphite. J. Appl. Cryst. 19, 200-1.

16. Gerward, L. (Private communication).

17. Skelton, E.F. (1984). High pressure research with synchrotron radiation. Physics Today, September 44-52.

18. Minomura, S. (editor). (1985). Solid State Physics under Pressure. Recent Advance with Anvil Devices. D. Reidel Publishing Company, Dotrecht.

19. Olsen, J.S., Buras, B., Gerward, L., Johansson, B., Lebech, B., Skriver, H. and Steenstrup, S. (1984). A new high-pressure phase and the equation of state of YbH_2. Physica Scripta 29, 503-507.

20. Benedict, U., Dabos, S., Gerward, L., Olsen, J.S., Beuers, J., Spirlet, J.C. and Dufour, C. (1987). Study of heavy-fermion compounds under high pressure. J. Magn. Magn. Mater. 63 & 63, 403-405.

21. Vohra, Y.K. Duclos, S.J. Ruoff, A.L. (1987). High pressure x-ray diffraction studies on rhenium up to 216 GPa (2.16 Mbar). Phys. Rev. B 36, 9790-2.

22. Prober, J., M. Prober and Schultz, J.M. (1975). Liquid Structure Analysis by Energy-Scanning X-Ray Diffraction: Merkury J. Appl. Cryst. 8, 405.

23. Ozawa, H. and Uno, R. (1986). Structural Study of Amorphous Lead Titanate by Energy-Dispersive X-Ray Diffraction Method. J. Appl. Cryst. 19, 395-399.

24. Hafner, J., Egami, T., Aur, S. and Giessen, B.C. (1987). The Structure of Calcium-Aluminium Glasses: X-ray Diffraction and Computer Simulation Studies. J. Phys. F: Met. Phys. 17, 1807-1815.

25. Minor, W., Schönfeld, B., Lebech, B., Buras, B. and Dmowski, W. (1987). Crystallization of Fe-Si-B metallic glasses studies by X-ray synchrotron radiation. J. Mater. Sci. 22, 4144.

Risø National Laboratory **Risø – M – 2751**

Title and author(s)

X-ray energy dispersive diffraction

Lecture notes

Bronislaw Buras

Date October 1988

Department or group
Physics

Groups own registration number(s)

Project/contract no.

Pages 37 Tables 1 Illustrations 17 References 25

ISBN 87-550-1470-4

Abstract (Max. 2000 char.)

X-ray energy dispersive diffraction is used mainly for structural characterization of polycrystalline powders and amorphous materials. One of the important features of it is the fixed scattering angle facilitating in particular studies of materials in special environments (e.g., high pressure, high and low temperature). There are two versions of x-ray energy dispersive diffraction. In one - called XED - an incident "white" beam is used and the spectral distribution of the diffracted photons is analyzed by means of a solid state detector. Its important feature is the simultaneous appearance of all reflections. In the other version - called monochromator scan method (MSM) - the incident beam is monochromatic and its wavelength is changed stepwise by rotating the crystal monochromator.

The lecture notes describe both versions and present examples of their applications.

Descriptors

Available on request from Risø Library, Risø National Laboratory, (Risø Bibliotek, Forskningscenter Risø),
P.O. Box 49, DK-4000 Roskilde, Denmark.
Telephone 02 37 12 12, ext. 2262. Telex: 43116, Telefax: 02 36 06 06

RR'350000 99

Available on exchange from:
Risø Library,
Risø National Laboratory,
P.O. Box 49, DK-4000 Roskilde, Denmark
Phone (02) 37 12 12 ext. 2262

ISBN 87-550-1470-4
ISSN 0418-6435